

Stability of the smectic phase in arrays of parallel quantum wires

Geo Jose and Bruno Uchoa

Center for Quantum Research and Technology, The University of Oklahoma, Norman, Oklahoma, 73071, USA

Using bosonization, we study a model of parallel quantum wires constructed from two dimensional Dirac fermions in the presence of periodic topological domain walls. The model accounts for the lateral spread of the wavefunctions ℓ in the transverse direction to the wires. The gapless modes confined to each domain wall are shown to form Luttinger liquids, which realize a well known smectic non-Fermi liquid fixed point when interwire Coulomb interactions are taken into account. Perturbative studies on phenomenological models have shown that the smectic fixed point is unstable towards a variety of phases such as superconductivity, stripe, smectic and Fermi liquid phases. Here, we show that the considered model leads to a phase diagram with only smectic metal and Fermi liquid phases. The smectic metal phase is stable in the ideal quantum wire limit $\ell \rightarrow 0$. For finite ℓ , we find a critical Coulomb coupling separating the strong coupling smectic metal from a weak coupling Fermi liquid phase. We conjecture that the absence of superconductivity should be a generic feature of similar models. We discuss the relevance of this model for quantum wires created with moire heterostructures.

I. INTRODUCTION

The low energy properties of gapless, interacting fermions in one dimension are generically described by the Luttinger liquid (LL) theory. The low energy excitations in this universality class are density waves, unlike quasiparticles in Fermi liquid theory in two or three dimensions [1, 2]. Arrays of parallel LL's have been studied extensively in the past thirty years with motivations such as the possibility of constructing higher dimensional non Fermi liquids and understanding the unusual normal state in cuprate superconductors [3–10]. Perturbations to the decoupled parallel LL arrays were generically shown to result in a higher dimensional Fermi liquid or an ordered state [11, 12]. It was then pointed out that one needs to include other marginal operators such as interwire density-density and current-current interactions in the most general fixed point action, which then describes a generalized smectic state [13]. The perturbative stability of the smectic fixed is now understood and leads to a rich, if generic, phase diagram, where the following phases can arise: *i*) smectic superconductor, *ii*) insulating stripe crystal, *iii*) Fermi liquid and *iv*) smectic metal state [13–15]. Very recently, this theory has been applied to the case of a triangular network of LL's [16] that emerge naturally in twisted bilayer graphene at marginal angles [17]. However, all these works are phenomenological. In this paper, we study an effective model within the formalism established by the hitherto mentioned works and examine what part of the generic phase diagram actually survives.

We first point out that moire heterostructures [18] offer a formidable platform for building arrays of identical and perfectly spaced quantum wires. The latter were recently realized in moire superlattices of twisted bilayer tungsten ditelluride (tWTe₂), which display parallel LL transport above 1.8K [19]. The distance between quantum wires is tunable by the interlayer twist angle. In general, application of a voltage difference between two layers in a van der Waals heterostructure (achievable by separately

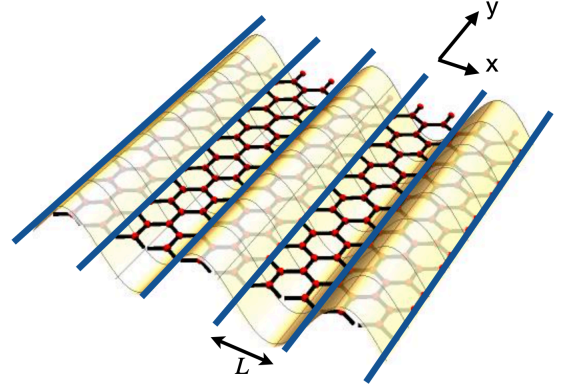


Figure 1. Cartoon representation of a periodic mass term (yellow wave form) on the honeycomb lattice. One dimensional modes at interfaces where the mass term changes sign are shown as thick blue lines. The transverse distance between these modes is L . The modes that live on the interface have a transverse width that dies off as $e^{-x^2/(2\ell^2)}$, with ℓ the lateral spread of the wavefunction (see text).

controlling the gates at each layer) permits theoretically integrating out the degrees of freedom in one of the layers. This results in an effective description for the other layer, that is affected by local potentials that modulate with the period of the moire pattern [20]. For tWTe₂, those local potentials make the bands flat along one direction, confining electrons along quasi-1D modes. In the case of moire heterostructures with Dirac fermions in each monolayer, as in marginally twisted graphene bilayers, those local potentials create periodic scalar, vector and mass terms [21–24]. A periodic mass term can confine Dirac fermions, with the lines where it changes sign forming quasi-1D modes that are topological. The periodic vector potential can be gauged away [25], and the scalar potential controlled with gating effects.

We construct an effective model for an array of parallel quantum wires using 2D Dirac fermions in the presence

of a periodically modulated mass term. This potential confines the low energy quasiparticles to propagate along one dimensional channels, as depicted in Fig. 1. Incorporating intra-wire Coulomb interactions, these modes are shown to be tunable LL's, akin to the domain wall modes found in gated bilayer graphene [26, 27], in mono and bilayer graphene under irradiation [28], and also in other contexts [25, 29, 30]. When inter-wire Coulomb interactions are taken into account, the model realizes a smectic metal state, whose Luttinger parameters can be obtained in terms of the fine structure constant of the material and the lateral confinement of the wavefunctions near the wires.

Even though the proposed model is topological, we suggest that it offers insight on the stability of the smectic phase for parallel quantum wires with non-topological origin, as in $t\text{WTe}_2$, and arrays of generic quantum wires with exponentially localized wavefunctions. This model naturally incorporates the lateral spread of the wavefunctions ℓ in the perpendicular direction to the quantum wires. Employing well established abelian bosonization methods to account for the possible instabilities to the smectic fixed point, we show that only two phases remain in this model: a smectic metal state and a 2D Fermi liquid state. We point out that, while the absence of the insulating smectic (stripe) phase is due to the lack of backscattering in the model, superconductivity is shown to be always an irrelevant (or marginal) perturbation at the smectic fixed point.

In the phase diagram, we find that the smectic metal and the Fermi liquid phases are separated by a quantum critical point set by a critical Coulomb coupling α_c , whose value is determined by the lateral spread ℓ normalized by the distance between the wires. For finite ℓ , the Fermi liquid phase is the leading instability in weak coupling ($\alpha < \alpha_c$), while the smectic metal is dominant in the strong coupling regime ($\alpha > \alpha_c$). The critical coupling vanishes in the ideal quantum wire limit ($\ell \rightarrow 0$), where the smectic phase is always dominant. We finally discuss the role of weak backscattering effects in similar models and suggest that the absence of superconductivity should be a general feature of quantum wires in moire heterostructures.

The paper is organized in the following way: in section II we describe the model of parallel quantum wires and derive the wavefunctions of their low energy modes. We then address the bosonized action of the quantum wires as tunable LLs, with the Luttinger parameters expressed in terms of the fine structure constant α and the lateral spread ℓ . We then write the action at the smectic metal fixed point once inter-wire Coulomb interactions are accounted for. In section III, we derive the phase diagram with the possible instabilities of the smectic fixed point according to this model, with a discussion about backscattering effects. Finally, in section IV we present our conclusions.

II. MODEL

We consider a generic continuum model of 2D Dirac fermions with two valley flavors, as in the honeycomb lattice. Generalizations to other physical lattices with Dirac quasiparticles and an arbitrary number of valleys are straightforward. In real space, the free Hamiltonian is

$$\mathcal{H}_0 = \int d^2r \sum_{\sigma} \Psi_{\sigma}^{\dagger}(\mathbf{r}) \hat{\mathcal{H}}_0(\mathbf{r}) \Psi_{\sigma}(\mathbf{r}), \quad (1)$$

where

$$\hat{\mathcal{H}}_0(\mathbf{r}) = \begin{pmatrix} \hat{\mathcal{H}}_+ & 0 \\ 0 & \hat{\mathcal{H}}_- \end{pmatrix} \quad (2)$$

is a 4×4 matrix defined in the two valleys $\alpha = \pm$,

$$\mathcal{H}_{\nu}(\mathbf{r}) = -iv\sigma_x\partial_x - i\alpha v\sigma_y\partial_y + M(\mathbf{r})\sigma_z, \quad (3)$$

with σ_x and σ_y the off diagonal Pauli matrices in the pseudospin space. $\Psi_{\sigma}(\mathbf{r})$ is a four-component spinor with spin $\sigma = \uparrow, \downarrow$. The mass term profile is taken to be of the form

$$M(\mathbf{r}) = M_0 \sin\left(\frac{\pi x}{L}\right), \quad (4)$$

which breaks the continuous translational symmetry along the x direction. It is well known in the context of the index theorem that real space lines where the mass term changes sign are topological, hosting zero energy modes [31]. The mass term (4) is a periodic function that changes sign at the nodal lines where $M(\mathbf{r}) = 0$, forming an array of parallel quantum wires with spacing L shown in Fig. 1.

Before addressing the fate of the possible many-body phases in this system, we first compute the zero-modes that live on these nodal lines. To solve for the eigenvalues and eigenvectors of $\mathcal{H}_+(\mathbf{r})$, it is convenient to linearize Eq. (4) in the vicinity of a zero-mass line at $x = 0$ to get

$$M(\mathbf{r}) \approx M_0 \frac{\pi x}{L}. \quad (5)$$

The eigenvalue problem can be solved analytically by performing two sequential unitary transformations in the pseudospin [32]: a rotation by $-\pi/2$ around the z axis, that takes $\sigma_x \rightarrow \sigma_y$ and $\sigma_y \rightarrow -\sigma_x$, followed by a rotation by $\pi/2$ around the y axis, which takes $\sigma_x \rightarrow -\sigma_z$ and $\sigma_z \rightarrow \sigma_x$. In the transformed basis, the “+” block of the eigenvalue problem

$$\mathcal{H}(\mathbf{r})\Psi(\mathbf{r}) = E\Psi(\mathbf{r}) \quad (6)$$

can be written as

$$\omega \begin{pmatrix} \ell k_y & -\partial_{\xi} + \xi \\ \partial_{\xi} + \xi & -\ell k_y \end{pmatrix} \Phi_+(\xi) = E_+ \Phi_+(\xi), \quad (7)$$

where we have introduced variables

$$\ell = \sqrt{\frac{vL}{M_0\pi}}, \quad (8)$$

$\omega = v/\ell$ and $\xi = x/\ell$. Eq. (7) implicitly assumes the ansatz

$$\Psi_+(\mathbf{r}) = \frac{e^{ik_y y}}{\sqrt{L_y}} \begin{pmatrix} \Phi_+(x) \\ \mathbf{0} \end{pmatrix} \quad (9)$$

due to translational symmetry in the y direction, with k_y the corresponding momentum and L_y the length of the quantum wires.

In this form, Eq. (7) resembles the problem of Dirac fermions in the presence of a uniform magnetic field [33], ℓ being the analogue of the magnetic length. Defining the ladder operator $\mathcal{O} = (\partial_\xi + \xi)/\sqrt{2}$ such that $[\mathcal{O}, \mathcal{O}^\dagger] = 1$ and the number operator $\hat{N} = \mathcal{O}^\dagger \mathcal{O}$, one can easily infer that the eigenvalues are given by

$$E_{+,N}^{(\pm)}(k_y) = \pm\omega\sqrt{\ell^2 k_y^2 + 2N}, \quad (10)$$

where $N = 1, 2, \dots$ indexing the gapped quantum wire modes, with the corresponding eigenvectors

$$\Phi_+^{N,\pm}(\xi) = \begin{pmatrix} \psi_N(x) \\ \pm\psi_{N-1}(x) \end{pmatrix}. \quad (11)$$

In a more explicit form,

$$\psi_N(x) = \frac{2^{-\frac{N}{2}}}{\pi^{\frac{1}{4}}\sqrt{N!}} e^{-x^2/(2\ell^2)} H_N(\xi), \quad (12)$$

where $H_N(\xi)$ is the N -th Hermite polynomial. The length ℓ hence determines the lateral spread of the wavefunctions confined to the quantum wires. The solution of the $\Psi_-(\mathbf{r})$ eigenmodes in the opposite valley is related by time-reversal operation,

$$\Psi_{-,N}^{(\pm)}(\mathbf{r}) = \frac{e^{-ik_y y}}{\sqrt{L_y}} \begin{pmatrix} \mathbf{0} \\ \Phi_-^{N,\pm}(\xi) \end{pmatrix}, \quad (13)$$

with $\Phi_-^{N,\pm}(\xi) = (\psi_N(x), \pm\psi_{N-1}(x))^T$. The “ \pm ” upper index accounts for the two particle-hole branches in each valley.

The $N = 0$ case corresponds to the gapless zero energy modes moving along the quantum wires. This case requires a more careful analysis to resolve the seeming ambiguity between particle and hole states in Eq. (10). In valley $\alpha = +$, the x dependent part of the wavefunction

$$\Psi_+(x) = \begin{pmatrix} \Phi_+^0(\xi) \\ \mathbf{0} \end{pmatrix} \quad (14)$$

gives the four-component eigenvector for a single right moving mode (per spin) with energy dispersion $E_+(k_y) = vk_y$. That can be seen by plugging in $\Phi_+^0(\xi)$ into (7) and explicitly solving the resulting differential equation. The zero energy mode $\Psi_-(x) = (\mathbf{0}, \Phi_-^0(\xi))^T$ in the opposite valley corresponds to a left moving mode with energy $E_-(k_y) = -vk_y$, as required by time reversal symmetry.

A. Tunable LLs

To derive an effective one dimensional model, we assume a suitable energy cut off $v\Lambda$ below the bulk mass M_0 and focus on the gapless modes propagating along the quantum wires. We closely follow the LL derivation in Ref. [26, 28]. In the infrared, we restrict our interest to the gapless modes with $N = 0$, with k_y the small momentum in the vicinity of the two valleys, αK . The field operator becomes

$$\hat{\chi}_\sigma(\mathbf{r}) = \frac{1}{\sqrt{L_y}} \sum_{\alpha=\pm} e^{i\alpha K y} \Psi_\alpha(x) \hat{\zeta}_{\alpha,\sigma}(y) \quad (15)$$

where $\hat{\zeta}_{\alpha,\sigma}(y) = \sum_{k_y} e^{ik_y y} \hat{\zeta}_{\alpha,\sigma,k_y}$ is a slowly varying field operator for electrons in valley α moving along the wire. The non-interacting Hamiltonian is given by

$$\mathcal{H}_0 = v \sum_{k_y, \sigma, \alpha} \alpha k_y \hat{\zeta}_{\alpha,\sigma}^\dagger(k_y) \hat{\zeta}_{\alpha,\sigma}(k_y). \quad (16)$$

The effective Coulomb interaction projected onto the one dimensional modes can be obtained by substituting (15) into the Coulomb interaction term

$$\mathcal{H}_{I,\text{intra}} = \frac{1}{2} \sum_{\sigma, \sigma'} \int_{\mathbf{r}, \mathbf{r}'} \hat{\rho}(\mathbf{r}) V(\mathbf{r} - \mathbf{r}') \hat{\rho}(\mathbf{r}'), \quad (17)$$

defined in terms of density operators

$$\hat{\rho}(\mathbf{r}) = \sum_{\sigma} \hat{\chi}_\sigma^\dagger(\mathbf{r}) \hat{\chi}_\sigma(\mathbf{r}). \quad (18)$$

Here, $V(\mathbf{r}) = e^2 e^{-r/\lambda}/(\epsilon r)$ is a screened Coulomb interaction, with the screening length λ set by metallic contacts with the wires and ϵ the background dielectric constant.

We note that the orthogonality of the spinors $\Psi_+(x)$ and $\Psi_-(x)$ suppresses backscattering in this model, unlike in conventional LLs. Since $\hat{\zeta}_{\alpha,\sigma}(y)$ are slow varying fields, the effective intra-wire interaction can be approximated by

$$\mathcal{H}_{I,\text{intra}} \approx \int_y \sum_{\alpha\beta} g_{\alpha\beta} \hat{\zeta}_{\alpha,\sigma}^\dagger(y) \hat{\zeta}_{\beta,\sigma'}^\dagger(y) \hat{\zeta}_{\beta,\sigma'}(y) \hat{\zeta}_{\alpha,\sigma}(y), \quad (19)$$

with

$$g_{\alpha\beta} = \frac{1}{2} \int_{x,x'} \int_{\bar{y}} V(x-x', \bar{y}) |\psi_0(x)|^2 |\psi_0(x')|^2, \quad (20)$$

where $\bar{y} = y - y'$. Using the standard g-ology notation in the LL literature, we denote $g_{+-} = g_{-+} = g_2$ and $g_{--} = g_{++} = g_4$, which turn out to be the same, $g_2 = g_4$. This is not a coincidence, but a manifestation of the chiral symmetry of the problem in the forward scattering terms. The equality between g_2 and g_4 also implies in the absence of current-current interaction terms [35].

In order to bosonize the fermionic Hamiltonian, we follow the abelian bosonization convention in Ref. [2, 13]. The fermionic fields for left and right moving modes

$$\hat{\zeta}_{\alpha,\sigma}(y) \sim e^{i\alpha\sqrt{\pi}[\phi_\sigma(y) - \alpha\theta_\sigma(y)]} \quad (21)$$

are cast in terms of the two bosonic fields $\phi_\sigma(y)$ and $\theta_\sigma(y)$. The Hamiltonian $\mathcal{H}_{\text{intra}} = \mathcal{H}_0 + \mathcal{H}_{I,\text{intra}}$ written in terms of charge (ρ) and spin (σ) variables exhibit spin-charge separation,

$$\mathcal{H}_{\rho,\sigma} = \frac{1}{2} \int dy \left[(\partial_y \Theta_{\rho,\sigma})^2 \frac{u_{\rho,\sigma}}{K_{\rho,\sigma}} + (\partial_y \Phi_{\rho,\sigma})^2 u_{\rho,\sigma} K_{\rho,\sigma} \right], \quad (22)$$

where

$$\Theta_{\rho,\sigma}(y) = \frac{1}{\sqrt{2}} [\theta^\uparrow(y) \pm \theta^\downarrow(y)] \quad (23)$$

and

$$\Phi_{\rho,\sigma}(y) = \frac{1}{\sqrt{2}} [\phi^\uparrow(y) \pm \phi^\downarrow(y)]. \quad (24)$$

The Luttinger parameters are given by $u_{\rho,\sigma} = v$, $K_\sigma = 1$ and

$$K_\rho = [1 + 2sg_4/(\pi v)]^{\frac{1}{2}}. \quad (25)$$

In the above, $s = 2$. In the case of spinless fermions, the spin part of $\mathcal{H}_{\text{intra}}$ is absent and $s = 1$. The LL stiffness in the charge sector K_ρ can be controlled by tuning the lateral spread of the wavefunctions ℓ through the coupling g_4 . The one dimensional modes that live on the nodal lines thus form a lattice of decoupled LLs.

B. Smectic metal

The density-density interaction between wires follows from $\mathcal{H}_{I,\text{intra}}$ after incorporating the wire index a for the superlattice into the wavefunctions and $\hat{\zeta}_{\alpha,\sigma}^a(y)$ operators, and hence into the definition of the field operators, $\hat{\chi}_{\sigma,a}(\mathbf{r}) = \sum_{\alpha=\pm} e^{i\alpha K y} \Psi_{\alpha,\sigma}(x_a) \hat{\zeta}_{\alpha,\sigma}^a(y)$, with $x_a \equiv x - X_a$ the relative coordinate to wire a . In line with [13–15], we only consider the coupling of charge densities between wires and not the exchange coupling, which is small when $\ell/L \ll 1$, with L the interwire distance. Thus,

$$\mathcal{H}_{\text{inter}} = \frac{1}{2} \sum_{a \neq a'} \int_{\mathbf{r}, \mathbf{r}'} V(\mathbf{r} - \mathbf{r}') \rho_a(\mathbf{r}) \rho_{a'}(\mathbf{r}'). \quad (26)$$

From the bosonization identities, we can write this as an effective one dimensional density density interaction,

$$\mathcal{H}_{\text{inter}} = \frac{2}{\pi} \int_y \sum_{a \neq a'} U_{a,a'} [\partial_y \Phi_{\rho,a}(y)] [\partial_y \Phi_{\rho,a'}(y)] \quad (27)$$

where

$$U_{a,a'} = \frac{1}{2} \int_{x,x',\bar{y}} V(x - x', \bar{y}) |\psi_0(x_a)|^2 |\psi_0(x'_a)|^2. \quad (28)$$

Thus only the charge sector is modified by the interwire interaction.

The action for the spin and charge degrees of freedom can be obtained by integrating out the $\Theta^{\rho,\sigma}$ fields. This yields

$$\mathcal{S}^\sigma = \int_{k,k_\perp,\omega} \frac{K^\sigma}{2} \left(\frac{\omega^2}{u_\sigma} + u^\sigma k^2 \right) |\Phi_\sigma(\mathbf{k})|^2 \quad (29)$$

$$\mathcal{S}^\rho = \int_{k,k_\perp,\omega} \frac{K^\rho(k_\perp)}{2} \left(\frac{\omega^2}{u^\rho(k_\perp)} + u^\rho(k_\perp) k^2 \right) |\Phi_\rho(\mathbf{k})|^2 \quad (30)$$

where $u^\sigma = v$, $K^\sigma = 1$, as before, and

$$\int_{k,k_\perp,\omega} \equiv L/(2\pi)^3 \int_{-\infty}^{\infty} d\omega dk \int_{-\pi/L}^{\pi/L} dk_\perp. \quad (31)$$

Luttinger parameters of the charge sector acquire momentum dependence from (27). Stability of the theory requires these parameters to be positive. We restrict the sum in (27) to nearest neighbor interactions as in [13]. This gives

$$\frac{u^\rho(k_\perp)}{K^\rho(k_\perp)} = v$$

$$u^\rho(k_\perp) K^\rho(k_\perp) = v + \frac{1}{\pi} 2sg_4 + \frac{1}{\pi} 4sV_1 \cos k_\perp L, \quad (32)$$

where $V_1 = U_{a'=a\pm 1}$, $\mathbf{k} = (\omega, k, k_\perp)$, $s = 2$. In the spinless case, $s = 1$ and the spin part of the action \mathcal{S}^σ is absent [34]. This phase is known as a smectic metal [13–15].

III. PHASE DIAGRAM

The stability of the smectic metal state to various instabilities has to be assessed via a renormalization group (RG) analysis of the relevant perturbations. Vast literature exist on the RG analysis of the smectic fixed point [13–15]. Therefore we do not repeat the analysis here, but adapt their RG equations to our model. The potentially relevant interactions in this case are nearest neighbor single electron tunneling (\mathcal{H}_t), nearest neighbor singlet pair (Josephson) tunneling (\mathcal{H}_{sc}), and the coupling between the charge density wave (CDW) order parameters. As mentioned before, due to the absence of backscattering, the interaction between CDW order parameters are absent in our model. The former two are given by

$$\mathcal{H}_t = \mathcal{T} \sum_{\alpha,\alpha'} \int dx \hat{\zeta}_{\alpha,\sigma}^{\dagger a} \hat{\zeta}_{\alpha,\sigma}^{a+1} + h.c. \quad (33)$$

$$\mathcal{H}_{sc} = \mathcal{J} \sum_{\alpha,\alpha'} \int dx \hat{\zeta}_{\alpha,\uparrow}^{\dagger a} \hat{\zeta}_{-\alpha,\downarrow}^{\dagger a} \hat{\zeta}_{\alpha',\downarrow}^{a+1} \hat{\zeta}_{-\alpha',\uparrow}^{a+1} + h.c., \quad (34)$$

where \mathcal{T} and \mathcal{J} are the single particle and Josephson tunneling amplitudes, respectively.

These perturbations become relevant when their scaling dimensions, $\eta_X = 2 - \Delta_X > 0$ for $X = t, sc$. These

scaling dimensions obtained from a one loop RG analysis in the spinless case are [36],

$$\Delta_{sc} = \int_{-\pi}^{\pi} \frac{dk_{\perp}}{2\pi} [2\kappa(k_{\perp})] (1 - \cos k_{\perp}) \quad (35)$$

$$\Delta_t = \frac{1}{4} \int_{-\pi}^{\pi} \frac{dk_{\perp}}{2\pi} 2 [\kappa(k_{\perp}) + \kappa^{-1}(k_{\perp})] (1 - \cos k_{\perp}), \quad (36)$$

where in the present model

$$\kappa(k_{\perp}) = \sqrt{\left(1 + \frac{2sg_4}{\pi v_F} + \frac{4sV_1}{\pi v_F} \cos k_{\perp}\right)}. \quad (37)$$

In the spinful case, $\Delta_{sc}^{\text{spin}} = 1 + \frac{1}{2}\Delta_{sc}$ and $\Delta_t^{\text{spin}} = \frac{1}{2} + \frac{1}{2}\Delta_t$.

We plot in Fig. 2 the regions where these perturbations are relevant as a function of fine structure constant, $\alpha_f = e^2/(\epsilon v)$ and the dimensionless lateral spread of the wavefunction in the wires, ℓ/L . We restrict the analysis to the regime $\ell/L \ll 1$, where the smectic action is stable. There is no part of the phase diagram where superconductivity is relevant [37]. It has been phenomenologically proposed that superconductivity may result in *active* environments, such as in high- T_c scenarios [38]. In the present model with screened Coulomb interactions, the minimum value of Δ_{sc} is 2, making it marginal at best. A similar conclusion is applicable to non-topological quantum wires with repulsive interactions whenever $g_4 \gg V_1$.

The curves in the plot describe the critical coupling α_c separating the regions where the smectic metal and the Fermi liquid phases emerge. As previously announced, the 2D Fermi liquid phase is the dominant instability in the weak coupling regime, when $\alpha_f < \alpha_c(\ell)$, whereas the smectic metal phase is the most relevant perturbation in strong coupling, $\alpha_f > \alpha_c(\ell)$. The quantum critical phase transition collapses in the $\ell \rightarrow 0$ limit, where $\alpha_c(\ell)$ scales to zero. That limit corresponds to the physical situation where the amplitude of the mass term in (4) $M_0 \gg vL$. The solid lines describe the spinless case, when the screening length $\lambda/L = 0.5$ (black triangles) and 1 (purple circles). The other two dashed curves correspond to the spinfull case for $\lambda/L = 0.5$ (blue squares) and 1 (orange diamonds).

The quantum wires described by this model remain generically stable in the regime where Coulomb repulsion (parametrized by the fine structure constant α_f) is strong enough, with the critical coupling α_c set by the lateral spread ℓ in the transverse direction to the wires. In the smectic metal phase, repulsive inter-wire interactions suppress single particle hopping between the wires, keeping the unidirectional flow of electrons stable. Conversely, when interactions are sufficiently weak ($\alpha_f < \alpha_c$), single particle tunneling becomes a relevant perturbation to the smectic metal, driving electrons to percolate across the quantum wires for any finite ℓ . In the latter regime, coherent unidirectional transport along the wires is destroyed in favor an isotropic 2D Fermi liquid.

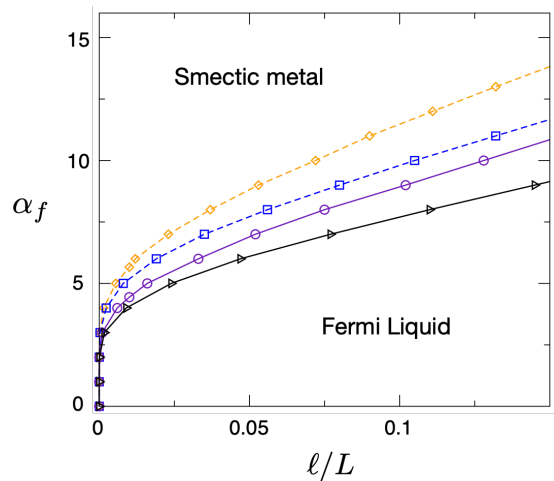


Figure 2. Fine structure constant $\alpha_f = e^2/(\epsilon v)$ vs lateral spread of the wavefunctions in the quantum wires, ℓ , normalized by the interwire separation L . Curves show the boundary between the Fermi liquid and smectic metal phases. Black triangles and purple circles: spinless particles for $\lambda/L = 0.5$ and 1, respectively. Blue square and orange diamonds: spinfull case for $\lambda/L = 0.5$ and 1, respectively. At finite lateral spread ℓ , there is a quantum phase transition separating the strong coupling smectic metal phase from the Fermi liquid one at weak coupling. At $\ell \rightarrow 0$, the quantum critical point collapses, and the smectic metal phase is always stable.

The proposed quantum phase transition can be experimentally explored through the control of the background dielectric constant of the substrate in the heterostructure where the wires are constructed [39]. We predict that dielectric materials could be suitably employed to push the system across the quantum phase transition.

A. Backscattering effects

Orthogonality between left and right modes eliminates backscattering in the present model. It is worth remarking that in a more general model, where there is backscattering, the phase diagram will comprise of regions where CDW coupling is the most relevant one. In lattice models with Dirac fermions, a finite but very small amount of backscattering is expected [26]. Backscattering is also expected in tWTe₂ bilayers and in layered van der Waals material NbSi_{0.45}Te₂ [40], where a non-symmorphic symmetry protects directional massless Dirac fermions that form equally spaced 1D channels in the bulk of the material, akin to stripes.

In the spinless case, it is well known that intra-wire backscattering can be rewritten as forward scattering term, thereby amounting only to a redefinition of the Luttinger parameters [1]. In the spinfull case, intra-wire backscattering is known to renormalize the Luttinger parameters and introduce an irrelevant perturbation (for repulsive interactions) in the spin channel [1, 2]. Backscat-

tering between quantum wires, however, can be relevant and may open a CDW gap at zero temperature. The coupling between wires has the form

$$\mathcal{H}_{cdw} = g_{cdw} \sum_{a,\alpha,\sigma,\sigma'} \int dx \hat{\zeta}_{\alpha,\sigma}^{\dagger a} \hat{\zeta}_{-\alpha,\sigma}^a \hat{\zeta}_{-\alpha,\sigma'}^{\dagger a+1} \hat{\zeta}_{\alpha,\sigma'}^{a+1}, \quad (38)$$

and can lead to a CDW state. From the lowest order RG analysis, this operator becomes relevant when $\eta_{cdw} = 2 - \Delta_{cdw} > 0$. For the spinless case, this is given by

$$\Delta_{cdw} = \int_{-\pi}^{\pi} \frac{dk_{\perp}}{2\pi} \left[2\kappa(k_{\perp})^{-1} \right] (1 - \cos k_{\perp}) \quad (39)$$

where $\kappa(k_{\perp})$ is defined in Eq. (37). For the spinful case, $\Delta_{cdw}^{\text{spin}} = 1 + \frac{1}{2}\Delta_{cdw}$.

The plot in Fig. 3 shows the regions in the zero temperature phase diagram where the operators corresponding to CDW, SC and Fermi liquid phases become relevant, as a function of the fine structure constant α_f and the ratio ℓ/L . In the model considered here, $g_{cdw} = 0$ due to orthogonality between left and right modes. In lattice models that can be approximated by the continuum model discussed before, g_{cdw} can be non-zero, although still small. In this scenario, the smectic metal phase may now give way for a more relevant CDW state at zero temperature.

In models where the backscattering term g_{cdw} is parametrically small compared to forward scattering terms g_2 and g_4 to begin with, the CDW gap is only observable at very small temperature. In the RG spirit, temperature plays a role of an infrared cut-off, where the RG flow stops. Since g_{cdw} is a marginal operator at the tree level ($g_2 = g_4 = 0$), it grows under the RG only logarithmically under rescaling of the momenta and fields,

$$g_{cdw}(T) = g_{cdw}(\Lambda_T) + \eta_{cdw} \ln \left(\frac{\Lambda_T}{T} \right), \quad (40)$$

where Λ_T is some ultraviolet temperature cut-off, with $g_{cdw}(\Lambda_T) \ll g_2, g_4$. Hence, g_{cdw} becomes dominant over forward scattering processes only near zero temperature, somewhere in the limit where $T/\Lambda_T \rightarrow 0$. There must be hence a low temperature T_* above which backscattering effects are subdominant, favoring either a smectic metal or Fermi liquid phases, even when backscattering is the most relevant perturbation. This seems to be the case in $t\text{WTe}_2$, where a smectic metal phase was observed down to 1.8K [19]. We predict that placing $t\text{WTe}_2$ on a dielectric substrate at fixed $T > T_*$ could destabilize the smectic metal towards a Fermi liquid phase.

The properties of those two phases, smectic metal and Fermi liquid, are rather well known. While the Fermi liquid state is the most general many particle state in two or three dimensions, the smectic metal state is a rather peculiar state of matter. In a smectic metal, there is large longitudinal conductivity in each quantum wire, but transport is incoherent in the transverse direction due to the irrelevance of inter-wire hopping.

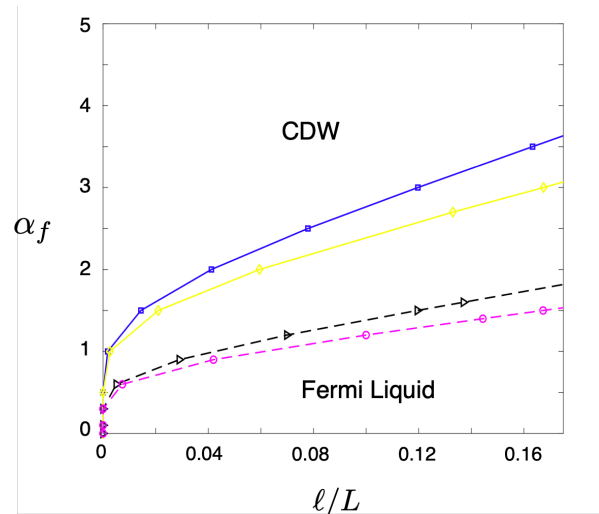


Figure 3. Zero temperature phase diagram in the presence of inter-wire backscattering. Black triangles and magenta circles: spinless particles for $\lambda/L = 0.5$ and 1 , respectively. Blue square and yellow diamonds: spinful case for $\lambda/L = 0.5$ and 1 , respectively. In models where inter-wire backscattering is parametrically small compared to forward scattering, the CDW phase can emerge only at very low temperature, even when the most relevant perturbation to the smectic metal fixed point (see text).

In the absence of disorder, resistivity along the wires $\rho_{yy} = 0$. Small amounts of disorder, which are present in realistic samples, can introduce backscattering and lead to a temperature dependence $\rho_{yy} \sim T^{\alpha_{\parallel}}$, where $\alpha_{\parallel} = \left[\int_{-\pi}^{\pi} \frac{dk_{\perp}}{2\pi} \kappa(k_{\perp})^{-1} \right] - 2$ [13, 15, 42]. On the other hand, in the transverse direction, conductivity is still given by a power law, $\sigma_{xx} \sim T^{\alpha_{\perp}}$, where the exponent α_{\perp} depends on the details of single particle hopping and Josephson couplings [15].

A few comments on the approximations used in our approach are in order. The continuum Dirac model employed here is known to be a very good approximation for the tight binding model of graphene at low energies. We focused on the lowest energy modes that arise in this model in the presence of a periodic mass term. In order to bosonize this model, we project the Coulomb interactions onto these modes. Previous studies have pointed out the deficiencies of the projected model, where processes that are ignored may become important at intermediate energy scales [44]. To the least, we expect the field theoretical approach used here to be a valid description of the asymptotic low-energy physics.

IV. CONCLUSION

We considered an effective model for an array of parallel quantum wires in 2D that accounts for the lateral spread of the wavefunctions ℓ in the transverse direction

to the wires. The model lacks backscattering, and does not lead to a stripe phase. Weak backscattering effects are expected to reintroduce a stripe phase at very low temperature, which we discuss in detail. Using standard abelian bosonization and RG methods, we calculated the Luttinger parameters of the sliding LL phase in terms of effective parameters of the Hamiltonian and analyzed what known instabilities of the smectic fixed point (previously found phenomenologically) actually survive. We showed that the smectic metal phase is stable in the ideal quantum wire limit ($\ell \rightarrow 0$), and survives at finite ℓ beyond a critical Coulomb coupling $\alpha_c(\ell)$ that grows monotonically with ℓ . In weak coupling ($\alpha < \alpha_c$), this model

describes a 2D Fermi liquid, with the wavefunctions in the quantum wires percolating over the whole system. We find that superconductivity is absent, a feature that is expected to be generic of similar models with Coulomb interactions.

V. ACKNOWLEDGEMENTS

GJ and BU thank Carl T. Bush Fellowship for support. BU thanks NSF grant DMR-2024864 for partial support.

-
- [1] T. Giamarchi, *Quantum Physics in One Dimension* (Oxford University Press, 2003).
- [2] E. Fradkin, *Field Theories of Condensed Matter Physics*, 2nd ed. (Cambridge University Press, 2013).
- [3] S. Strong, D. G. Clarke, and P. W. Anderson, Magnetic Field Induced Confinement in Strongly Correlated Anisotropic Materials, *Phys. Rev. Lett.* **73**, 1007 (1994).
- [4] P. W. Anderson, “Confinement” in the one-dimensional Hubbard model: Irrelevance of single-particle hopping, *Phys. Rev. Lett.* **67**, 3844 (1991).
- [5] J. M. Tranquada, D. J. Buttrey, V. Sachan, and J. E. Lorenzo, Simultaneous Ordering of Holes and Spins in $\text{La}_2\text{NiO}_{4.125}$, *Phys. Rev. Lett.* **73**, 1003 (1994).
- [6] J. Zaanen and O. Gunnarsson, Charged magnetic domain lines and the magnetism of high- T_c oxides, *Phys. Rev. B* **40**, 7391 (1989).
- [7] K. Machida, Magnetism in La_2CuO_4 based compounds, *Phys. C Supercond.* **158**, 192 (1989).
- [8] M. Kato, K. Machida, H. Nakanishi, and M. Fujita, Soliton Lattice Modulation of Incommensurate Spin Density Wave in Two Dimensional Hubbard Model -A Mean Field Study-, *J. Phys. Soc. Japan* **59**, 1047 (1990).
- [9] V. J. Emery, S. A. Kivelson, and J. M. Tranquada, Stripe phases in high-temperature superconductors, *Proc. Natl. Acad. Sci. USA* **96**, 8814 (1999).
- [10] R. Mukhopadhyay, C. L. Kane, and T. C. Lubensky, Crossed sliding Luttinger liquid phase, *Phys. Rev. B* **63**, 081103(R) (2001).
- [11] See V. Emery, in *Highly Conducting One-Dimensional Solids*, edited by J. Devreese et al. (Plenum, New York, 1979).
- [12] C. Bourbonnais and L. G. Caron, Renormalization Group Approach To Quasi-One-Dimensional Conductors, *Int. J. Mod. Phys. B* **5**, 1033 (1991).
- [13] V. J. Emery, E. Fradkin, S. A. Kivelson, and T. C. Lubensky, Quantum Theory of the Smectic Metal State in Stripe Phases, *Phys. Rev. Lett.* **85**, 2160 (2000).
- [14] A. Vishwanath and D. Carpentier, Two-Dimensional Anisotropic Non-Fermi-Liquid Phase of Coupled Luttinger Liquids, *Phys. Rev. Lett.* **86**, 676 (2001).
- [15] R. Mukhopadhyay, C. L. Kane, and T. C. Lubensky, Sliding Luttinger liquid phases, *Phys. Rev. B* **64**, 045120 (2001).
- [16] C. Chen, A. H. Castro Neto, and V. M. Pereira, Correlated states of a triangular net of coupled quantum wires: Implications for the phase diagram of marginally twisted bilayer graphene, *Phys. Rev. B* **101**, 165431 (2020).
- [17] S. G. Xu *et al.*, Giant oscillations in a triangular network of one-dimensional states in marginally twisted graphene, *Nat. Comm.* **10**, 4008 (2019).
- [18] E. Y. Andrei, D. Efetov, P. Jarillo-Herrero, A. H. MacDonald, K. F. Mak, T. Senthil, E. Tutuc, A. Yazdani, and A. F. Young, The marvels of moiré materials, *Nat. Rev. Mater* **6**, 201 (2021).
- [19] P. Wang, G. Yu, Y. H. Kwan, *et al.*, One-dimensional Luttinger liquids in a two-dimensional moiré lattice, *Nature* **605**, 57–62 (2022).
- [20] M. Kindermann and P. N. First, Local sublattice-symmetry breaking in rotationally faulted multilayer graphene, *Phys. Rev. B* **83**, 045425 (2011).
- [21] B. Uchoa, V. N. Kotov, and M. Kindermann, Valley order and loop currents in graphene on hexagonal boron nitride, *Phys. Rev. B* **91**, 121412(R) (2015).
- [22] M. Yankowitz, J. Xue, D. Cormode, J. D. Sanchez-Yamagishi, K. Watanabe, T. Taniguchi, P. Jarillo-Herrero, P. Jacquod, and B. J. LeRoy, Emergence of superlattice Dirac points in graphene on hexagonal boron nitride, *Nat. Phys.* **8**, 382 (2012).
- [23] W. Yang, G. Chen, Z. Shi, C.-C. Liu, L. Zhang, G. Xie, M. Cheng, D. Wang, R. Yang, D. Shi, K. Watanabe, T. Taniguchi, Y. Yao, Y. Zhang, and G. Zhang, Epitaxial growth of single-domain graphene on hexagonal boron nitride, *Nat. Mater.* **12**, 792 (2013).
- [24] B. Sachs, T. O. Wehling, M. I. Katsnelson, and A. I. Lichtenstein, Adhesion and electronic structure of graphene on hexagonal boron nitride substrates, *Phys. Rev. B* **84**, 195414 (2011).
- [25] M. Kindermann, B. Uchoa, and D. L. Miller, Zero-energy modes and gate-tunable gap in graphene on hexagonal boron nitride, *Phys. Rev. B* **86**, 115415 (2012).
- [26] M. Killi, Tzu-Chieh Wei, I. Affleck, and A. Paramekanti, Tunable Luttinger Liquid Physics in Biased Bilayer Graphene, *Phys. Rev. Lett.* **104**, 216406 (2010).
- [27] I. Martin, Y. M. Blanter, and A. F. Morpurgo, Topological Confinement in Bilayer Graphene, *Phys. Rev. Lett.* **100**, 036804 (2008).
- [28] S. Biswas, T. Mishra, S. Rao, and A. Kundu, Chiral Luttinger liquids in graphene tuned by irradiation, *Phys. Rev. B* **102**, 155428 (2020).

- [29] A. J. Heeger *et al.*, Solitons in conducting polymers, Rev. Mod. Phys. **60**, 781 (1988).
- [30] G. W. Semenoff, V. Semenoff, and F. Zhou, Domain Walls in Gapped Graphene, Phys. Rev. Lett. **101**, 087204 (2008).
- [31] R. Jackiw and C. Rebbi, Solitons with fermion number $1/2$, Phys. Rev. D **13**, 3398 (1976).
- [32] S. Tchoumakov, V. Jouffrey, A. Inhofer, E. Bocquillon, B. Plaçais, D. Carpentier, M. O. Goerbig, Volkov-Pankratov states in topological heterojunctions, Phys. Rev. B **96**, 201302 (2017).
- [33] A. H. Castro Neto, F. Guinea, N. M. R. Peres, K. S. Novoselov, and A. K. Geim, The electronic properties of graphene, Rev. Mod. Phys. **81**, 109 (2009).
- [34] In comparison with the notation in [13], $\left(\frac{u^\rho(k_\perp)}{K^\rho(k_\perp)}\right)^{-1} = W_0(k_\perp)$ and $u^\rho(k_\perp)K^\rho(k_\perp) = W_1(k_\perp)$. The parameter that decides the phase diagram is $\kappa = \sqrt{W_0(k_\perp)W_1(k_\perp)}$.
- [35] The Coulomb term can be cast in terms of charge and current density terms $j_\mu(\mathbf{r})W_\mu(\mathbf{r} - \mathbf{r}')j_\mu(\mathbf{r}')$, where $j_0 = \rho_+ + \rho_-$ is a charge density and $j_1(\mathbf{r}) = \rho_+ - \rho_-$ the current density. When $g_2 = g_4$ the current-current term is zero.
- [36] Notice that, for the spinless case here there is an extra factor of 2, compared to [13]. This is because we consider a spinless case as opposed to the spin gapped case considered in high- T_c like scenarios.
- [37] One could in principle consider the Josephson coupling between next-nearest neighbor and so on after including the same number of terms in (32). We have checked that *sc* coupling for the next nearest neighbor is even less relevant.
- [38] V. J. Emery, S. A. Kivelson, and O. Zachar, Spin-gap proximity effect mechanism of high-temperature superconductivity, Phys. Rev. B **56**, 6120 (1997).
- [39] M. Kim, *et al.*, Control of electron-electron interaction in graphene by proximity screening, Nat. Commun. **11**, 2339 (2020).
- [40] T. Y. Yang, *et al.*, Directional massless Dirac fermions in a layered van der Waals material with one-dimensional long-range order, Nat. Materials **19**, 27 (2020).
- [41] Umklapp interactions are relevant for repulsive interactions and can open a CDW gap (see Ref.). These have a non-zero amplitude only precisely at half filling and can be ignored in experimental settings where the chemical potential can be tuned at will.
- [42] A. Luther and I. Peschel, Fluctuation Conductivity and Lattice Stability in One Dimension, Phys. Rev. Lett. **32**, 922 (1974).
- [43] V. M. Pereira, A. H. Castro Neto, and N. M. R. Peres, Tight-binding approach to uniaxial strain in graphene, Phys. Rev. B **80**, 045401 (2009).
- [44] Meden, V., Metzner, W., Schollwöck, U. et al. Luttinger liquids with boundaries: Power-laws and energy scales, Eur. Phys. J. B **16**, 631–646 (2000)